

Superpriming of synaptic vesicles as a common basis for intersynapse variability and modulation of synaptic strength

Holger Taschenberger^{a,b}, Andrew Woehler^{b,c}, and Erwin Neher^{b,c,1}

^aDepartment of Molecular Neurobiology, Max Planck Institute of Experimental Medicine, 37075 Göttingen, Germany; ^bCenter for Nanoscale Microscopy and Molecular Physiology of the Brain, 37073 Göttingen, Germany; and ^cEmeritus Group Membrane Biophysics, Max Planck Institute for Biophysical Chemistry, 37077 Göttingen, Germany

Contributed by Erwin Neher, June 10, 2016 (sent for review April 21, 2016; reviewed by William Betz and Bert Sakmann)

Glutamatergic synapses show large variations in strength and short-term plasticity (STP). We show here that synapses displaying an increased strength either after posttetanic potentiation (PTP) or through activation of the phospholipase-C-diaclyglycerol pathway share characteristic properties with intrinsically strong synapses, such as (i) pronounced short-term depression (STD) during high-frequency stimulation; (ii) a conversion of that STD into a sequence of facilitation followed by STD after a few conditioning stimuli at low frequency; (iii) an equalizing effect of such conditioning stimulation, which reduces differences among synapses and abolishes potentiation; and (iv) a requirement of long periods of rest for reconstitution of the original STP pattern. These phenomena are quantitatively described by assuming that a small fraction of “superprimed” synaptic vesicles are in a state of elevated release probability ($p \sim 0.5$). This fraction is variable in size among synapses (typically about 30%), but increases after application of phorbol ester or during PTP. The majority of vesicles, released during repetitive stimulation, have low release probability ($p \sim 0.1$), are relatively uniform in number across synapses, and are rapidly recruited. In contrast, superprimed vesicles need several seconds to be regenerated. They mediate enhanced synaptic strength at the onset of burst-like activity, the impact of which is subject to modulation by slow modulatory transmitter systems.

posttetanic potentiation | short-term plasticity | calyx of Held | Munc13 | phorbol ester

Glutamatergic synapses display a variety of dynamic changes in response to stimulation with action potential (AP) trains, ranging from immediate short-term depression to facilitation followed by depression (1). Both pharmacological (2–6) and molecular (7–9) perturbations have been described, which change such patterns from one to the other in a given synapse. Short-term plasticity (STP) has been shown to underlie many basic signal processing tasks of circuits in the central nervous system (10–13) and rapid changes of STP have been considered “... to be an almost necessary condition for the existence of (short-lived) activity states in the central nervous system” (ref. 14, p. 247). The balance between facilitation and depression is shifted during posttetanic potentiation (PTP) (15) and behavioral states are dynamically regulated by STP (16). Regulation occurs through slow, modulatory transmitter systems (17, 18). However, many open questions regarding the mechanisms underlying such changes remain. Modulation of presynaptic voltage-gated Ca^{2+} channels by slow transmitter systems is probably the most powerful mechanism of changing release probability (p) of synaptic vesicles (SVs) (19–21). Changes in intrinsic $[\text{Ca}^{2+}]_i$; sensitivity of the release apparatus also contribute and have been investigated in the context of the phospholipase-C-diaclyglycerol (PLC-DAG) signaling pathway (22–26) and posttetanic potentiation (15, 27–30), but the influence of this modulation on STP is less well understood.

Here, we describe heterogeneity of STP among synapses in the medial nucleus of the trapezoid body (MNTB)—the calyces of Held. AP-evoked excitatory postsynaptic currents (EPSCs) vary in amplitude

by more than a factor of 5 among calyx synapses and display divergent STP patterns (31). We show that such variability is similar to differences that can be experimentally induced by application of the DAG analog phorbol 12,13-dibutyrate (PdBu) and we explore the hypothesis that intrinsic heterogeneity of synaptic strength among synapses is caused by different degrees of activation of the PLC-DAG pathway, possibly due to the action of slow modulatory transmitter systems. We find that the very pronounced heterogeneity in p and synaptic strength among resting synapses rapidly vanishes during repetitive AP firing, such that EPSCs at steady state (EPSC_{ss}) become very similar, both during high-frequency stimulation and after conditioning with low-frequency trains. The remaining variability observed under such conditions shows very little correlation with the pronounced synapse to synapse variability of the initial EPSCs (EPSC_1). Last but not least we find that EPSCs augmented by PTP share many features with those potentiated by PdBu application or by intrinsic modulation—in particular, a rapid loss of potentiation during repetitive stimulation.

We show that these findings can be quantitatively explained by a model, which assumes that resting synapses are endowed with a variable fraction of SVs, typically about 20–40%, that are in a “superprimed” state of elevated p (32). Application of PdBu or induction of PTP substantially increases the fraction of superprimed SVs and thereby the average p . During repetitive stimulation, responses of different synapses become more and more similar because superprimed SVs are consumed early, leaving normally primed SVs behind. Superpriming is a slow process, taking several seconds. It generates SVs with high p whereas normal priming is fast and supplies SVs with low p .

Significance

Short-term plasticity (STP) of synaptic connections underlies many basic signal processing capabilities of the brain, such as gain control, temporal filtering, and adaptation. Glutamatergic synapses, the predominant excitatory synapses in the brain, display large variability both in basal synaptic strength and in STP. We show that a small fraction of release-ready vesicles are released with much higher probability than other vesicles. The number of these “superprimed” vesicles is variable among synapses, but increases strongly after application of phorbol ester, an analogue of the second messenger diacylglycerol, and after inducing posttetanic potentiation. Thus, modulatory transmitter systems, acting through the phospholipase-C-diaclyglycerol pathway, will be able to upregulate superprimed vesicles and thereby boost synaptic strength at the onset of burst-like activity.

Author contributions: E.N. designed research; H.T. and A.W. performed research; H.T., A.W., and E.N. analyzed data; and H.T., A.W., and E.N. wrote the paper.

Reviewers: W.B., University of Colorado School of Medicine; and B.S., Max Planck Institute of Neurobiology.

The authors declare no conflict of interest.

Freely available online through the PNAS open access option.

¹To whom correspondence should be addressed. Email: eneher@gwdg.de.

This article contains supporting information online at www.pnas.org/lookup/suppl/doi:10.1073/pnas.1606383113/-DCSupplemental.

that maintain synaptic responses during sustained stimulation. Slow superpriming induced by activation of the PLC-DAG pathway has been observed before in the calyx of Held under voltage clamp, using step depolarizations (33). In hippocampal synapses, superpriming was shown to depend on the presence of at least one isoform of rab3 (32). We discuss our data in terms of a parallel SV pool model, in which normally primed and superprimed SVs reach their release-ready state independently. However, our data are equally compatible with a sequential process during which primed SVs mature to reach the superprimed state. We stress that the distinction between normally primed and superprimed SVs is not related to the previously described pools of slow and fast SVs at the calyx of Held (34). Rather, our data on AP-evoked EPSCs presented here demand that the latter needs to be subdivided, to accommodate normally primed and superprimed vesicles, respectively.

Results

Heterogeneity Among Release-Ready SVs. Calyces of Held represent a well-defined and homogenous population of axosomatic synapses that are thought to function as simple sign-inverting relays. For the majority of our experiments (Figs. 1–5) we stimulated afferent axons giving rise to calyx terminals and recorded AP-evoked EPSCs, using acute brainstem slices from P13–16 rats, as described previously (35). Some experiments were also performed using cultured hippocampal neurons (Fig. 6). When recording from voltage-clamped MNTB principal neurons and comparing EPSCs of different calyx synapses in response to trains of afferent fiber stimuli at frequencies ≥ 50 Hz, we can observe marked differences in their short-term plasticity. Fig. 1 gives three examples: One synapse shows pronounced depression at 50 Hz, 100 Hz, and 200 Hz (Fig. 1A); another synapse shows depression at 50 Hz, although with indications of some facilitation, superimposed onto depression for both 100 Hz and 200 Hz (Fig. 1B); and a third synapse shows pronounced net facilitation initially, followed by depression (Fig. 1C). In these examples the synapse with the strongest depression had the largest EPSC₁. When responses recorded from 23 synapses under identical conditions are analyzed with respect to their EPSC₁ and paired-pulse ratios (PPRs), a scatter plot of these two parameters shows a prominent correlation (Fig. 2, symbols with light colors). Such behavior has been described for other glutamatergic synapses before (36–38) and is generally interpreted in the sense that synapses with large EPSC₁ have high p , which leads to substantial depletion of SVs already during the first few EPSCs.

Differential Slow Modulation of p as a Likely Basis of Heterogeneity.

Some morphological variability seen among calyces of older mice (P16–19) has been reported to correlate with functional parameters

(31). Here we explore possible mechanisms that generate functional heterogeneity among calyces. We considered that there may be constitutively active modulatory influences by slow transmitter systems (17, 18), which affect individual synapses differently. Many such influences operate through signaling pathways involving PLC and DAG. The DAG analog PdBu has been shown to increase EPSCs by a factor of 2–5 at the calyx (22, 23), mainly by increasing p . We therefore compared synaptic strength and STP in calyx synapses before and after application of PdBu. The set of 23 synapses analyzed in Fig. 2 includes seven cells, for which EPSCs were recorded both under control conditions (symbols with light colors) and after application of 1 μ M PdBu (symbols with dark colors). Strikingly, EPSCs recorded in the presence of PdBu follow the same relationship between PPR and EPSC₁ as seen under control conditions, extending the plot toward more than two times larger EPSC₁. This finding suggests that similar processes may generate the heterogeneity of synaptic strength among individual calyx synapses and the potentiation of EPSCs by PdBu.

Another more surprising observation is that the heterogeneity, which is observed among rested synapses, quickly vanishes during repetitive high-frequency stimulation. Likewise, potentiation induced by application of PdBu quickly diminishes during EPSC trains. Fig. 3A compares two synapses (blue and red), selected to represent large differences in EPSC size. They were stimulated at a frequency of 200 Hz, both under control conditions (open symbols) and during application of 1 μ M PdBu (solid symbols). Despite a more than fivefold difference in EPSC₁, the amplitudes converge to a similar steady state (EPSC_{ss}) during repetitive high-frequency stimulation. This convergence does not approach zero, as seen in Fig. 3A, *Inset*, where the late sections of the EPSC trains are shown at expanded amplitude scale. Plotting EPSC_{ss} against EPSC₁ for 200-Hz trains recorded in the larger sample of 23 synapses shows that there is little correlation between these two quantities (Fig. 3C, bottom trace, blue symbols). This plot includes both control (open symbols) and PdBu data (solid symbols) together with a fit to the combined datasets. If the sets are fitted separately, very similar regression lines with small slopes (0.014 ± 0.014 for control and 0.012 ± 0.01 for PdBu) are obtained. This result, again, points toward similar mechanisms underlying both endogenous heterogeneity and PdBu potentiation.

At the calyx of Held, potentiation of neurotransmitter release by 1-oleoyl-2-acetyl-sn-glycerol (OAG), a more physiological substitute for PdBu, has been interpreted as a slow maturation process of SVs, following their recruitment to the readily releasable pool (33). This process was found to display distinct pharmacology, involving PLC and DAG, and to take several seconds for completion. Likewise superpriming, described by Schlüter et al. in hippocampal neurons (32), was

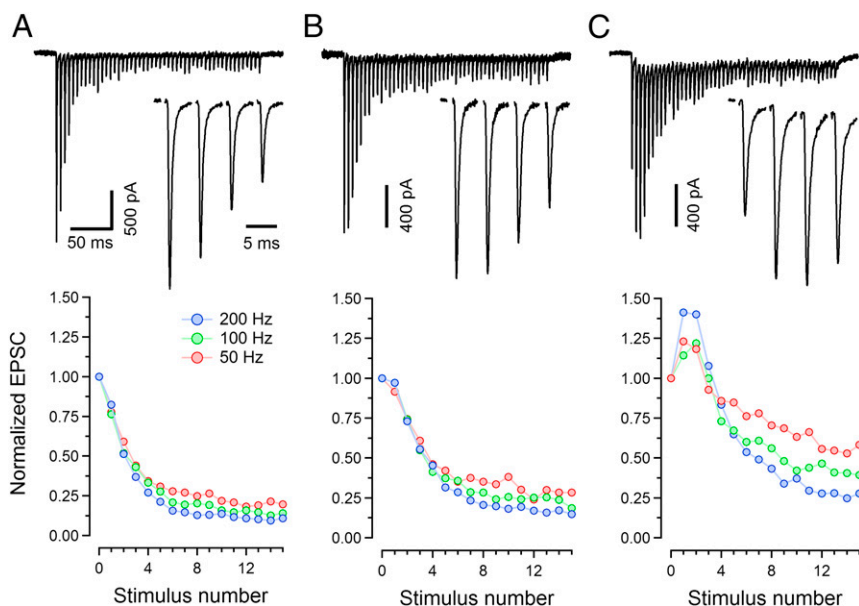


Fig. 1. Variability of short-term plasticity among calyx synapses. (A–C, *Upper*) Sample EPSC trains recorded in three different calyx synapses (P13–15) in response to high-frequency afferent fiber stimulation (200 Hz, 50 stimuli). *Insets* in A–C show the initial 4 EPSCs of the trains at a faster timescale. The bath solution contained 2 mM Ca²⁺ and 1 mM kynurenic acid for all experiments illustrated here and in Figs. 2–5. (A–C, *Lower*) Average EPSC amplitudes of the same synapses for three different frequencies (50 Hz, 100 Hz, and 200 Hz) were calculated from three to four repetitions and plotted against stimulus number. For clarity, only the initial 15 EPSC amplitudes are plotted.

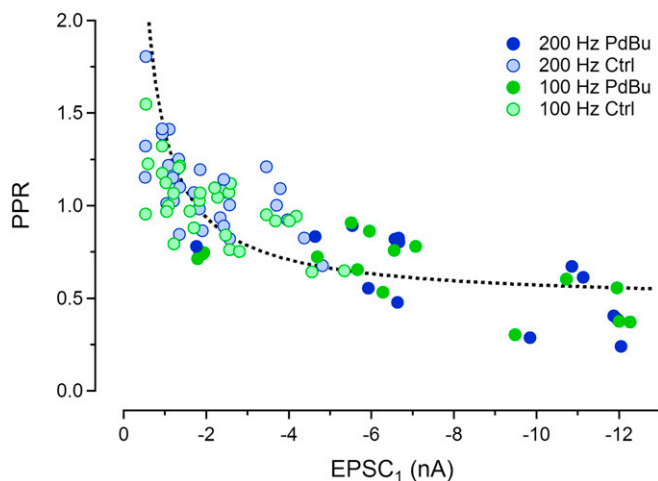


Fig. 2. Paired-pulse ratios plotted as a function of EPSC₁. EPSCs were measured in response to 100 Hz (green) and 200 Hz (blue) stimulus trains. Symbols with light colors represent EPSCs recorded under control conditions, and symbols with dark colors represent EPSCs recorded in the presence of 1 μ M PdBu. The dashed curve shows the prediction of a simple model as described in *SI Text*.

found to be slow to recover after high-frequency stimulation. We reasoned that the slowness of superpriming may be the cause for both the convergence of EPSC amplitudes of different synapses and the collapse of PdBu-induced potentiation during repetitive stimulation. Late in a high-frequency train, SVs are newly recruited and consumed in rapid succession. Thus, only a minority of released SVs will be superprimed, if superpriming is slower than normal priming. We therefore stimulated the same two synapses illustrated in Fig. 3*A* at 2 Hz to allow more time for superpriming in between stimuli (Fig. 3*B*). As expected, steady-state EPSCs at 2-Hz stimulation mirrored to a large extent the differences in EPSC₁. Scatter plots of EPSC_{ss} vs. EPSC₁ at lower frequencies (Fig. 3*C*) show distinct correlations between the two quantities, which are stronger, the lower the frequencies. In Fig. 3*C*, each symbol (color coded for frequency) represents one synapse at that frequency. Data points for a given frequency from different synapses are well approximated by straight dashed lines. In all cases, data obtained in the presence of PdBu (solid symbols) are perfectly consistent with those obtained under control conditions (open symbols), strengthening the notion that endogenous variations among resting synapses and potentiation induced by PdBu application are generated by the same mechanism.

The line fits for 100-Hz and lower stimulus frequencies converge at x and y values near -0.5 nA (Fig. 3*C*, *Inset*). Assuming that EPSCs reflect a sum of contributions from normally primed SVs (SV_ns) and superprimed SVs (SV_ss), this convergence finds an appealing interpretation: SV_ns uniformly contribute about -0.5 nA to EPSC₁ in all synapses. An additional EPSC component that is variable in amplitude among different synapses is contributed by SV_ss. A formal treatment of such a “parallel pool model” is provided in *SI Text*. For such a model, synapses with increasing contributions of SV_ss to the EPSC move up along the line fit of the scatter plot. Given the mean EPSC₁ of -1.78 nA and assuming the contribution of SV_ns to be about -0.5 nA, we conclude that SV_ss contribute an average of -1.28 nA. However, because of the approximately 5 times higher release probability, the number of release-ready SV_ss needs to be only 0.51 times that of SV_ns to contribute -1.28 nA to the EPSC. Thus, we may conclude that SV_ss account for approximately one-third of all primed vesicles. The slope of the ($\Delta y/\Delta x$) plot reports the ratio of EPSC_{ss} over EPSC₁ for the SV_s component. According to the model, the slope depends only on the SV_s component and thus provides valuable information about superpriming. Ratios of EPSC_{ss} over EPSC₁ are commonly used to quantify short-term depression (STD), although they may be influenced by facilitation (increase in p) and by desensitization. We therefore refer to the slope for a given frequency as depression (STD) of the SV_s component, keeping in mind that this may represent a simplification.

Our finding that such data for several frequencies and across many cells, both for control and in the presence of PdBu, can well be approximated by straight converging lines can be taken as evidence that (i) synaptic responses have a SV_n component, which is similar among individual synapses and displays little STD for stimulus frequencies of 0.5–50 Hz; (ii) there is an additional, variable component contributed by SV_ss displaying strong STD even at low frequencies; and (iii) PdBu predominantly modulates the variable SV_s component. A simple two-pool model corroborates these conclusions in a quantitative way (*SI Text*).

Time Course of Consumption of the SV_s Component and Its Frequency Dependence.

Assuming that SV_s and SV_n contributions to EPSCs are additive and that the latter is relatively uniform among individual synapses, it is straightforward to determine the time course of the SV_s contribution during stimulus trains by forming differences between EPSC amplitudes obtained in synapses with either high or low contributions of SV_s to the EPSCs (32). We refined this approach by allowing for the fact that SV_n components may not be exactly the same for high-SV_s and low-SV_s synapses due to cell-to-cell variations. Thus, we did not subtract the entire low-SV_s response from the high-SV_s response, but a fraction of it. The criterion for selecting the fraction (usually very close to 1) was that the resulting EPSC component contributed by SV_ss has a depression ratio, determined by the slope in Fig. 3*C*, which is 0.036 ± 0.008 for 100-Hz stimulation. Fig. 4*A* shows three examples of such amplitude time courses, normalized to an initial value of 1 (green traces, right ordinate) and an exponential fit to their average (black dashed curve). These traces are normalized because the absolute amplitudes unfortunately do not provide information about the sizes of the SV_s pools of individual synapses, but report only differences (details in Fig. 4 legend). Nevertheless, we can calculate the release probability of SV_s (p_s) because it is the ratio of EPSC₁ over pool size, for which absolute pool sizes cancel out. To do so, we calculated normalized SV_s pool size by back extrapolation of a linear fit to the cumulative version of the normalized average time course of Fig. 4*A* (red traces), as described previously (39, 40). The SV_s pool size was found to be 1.99 ± 0.02 (in units of EPSC₁). Thus, EPSC₁ consumes a fraction of $1/1.99$ of the SV pool, corresponding to $p_s = 0.497 \pm 0.005$ (note that here and in the following text subscripts, s and n are used for denoting parameters for superprimed and normally primed vesicles, respectively).

Another p_s estimate can be obtained from the time constant of an exponential fit to the average decay time course of the component contributed by SV_ss to each EPSC during trains (Fig. 4*A*). For a simple depletion model (*SI Text*) the time constant τ_s of approach to steady state is determined by both p_s and the priming rate constant. Its inverse is just the sum of both quantities, if τ_s and priming rate constant are measured in units of the interstimulus interval (ISI). For a SV pool, which depletes almost completely—such as the SV_s pool during 100-Hz stimulation—the priming is slow, relative to SV consumption, and therefore p_s is close to $1/\tau_s$. The exponential fit to the average time course shown in Fig. 4*A* has a decay $\tau_s = 1.43 \pm 0.08$ ISIs, corresponding to $p_s = 0.70 \pm 0.04$. This value is significantly larger than the p_s estimated from EPSC₁ and SV_s pool size above (0.497 ± 0.005). This difference is most likely due to facilitation building up during the stimulus train, because the exponential fit describes the approach to steady state toward the end of the EPSC trains, whereas the first estimate was largely based on EPSC₁. Taking the ratio of the two p_s estimates, we may conclude that facilitation, expressed as an increase in p_s , enhances release by a factor of 1.41.

In Fig. 4*B* we explore the frequency dependence of the steady state of the SV_s component. Slopes of line fits of Fig. 3*C* are plotted against the logarithm of stimulus frequency. We discuss these slopes, which are ratios of steady-state over initial amplitudes of the isolated SV_s components, in terms of the abovementioned parallel pool model. The model assumes that a given pool of SVs is consumed at a rate constant proportional to p and stimulus frequency. This pool is refilled with rate constant k_+ . The size of it is assumed to be variable among synapses and modulated by PdBu or by induction of PTP. In addition to the SV_s pool, there is a fixed-size SV_n pool, the properties of which are further discussed below (*SI Text*). Disregarding possible effects of facilitation and

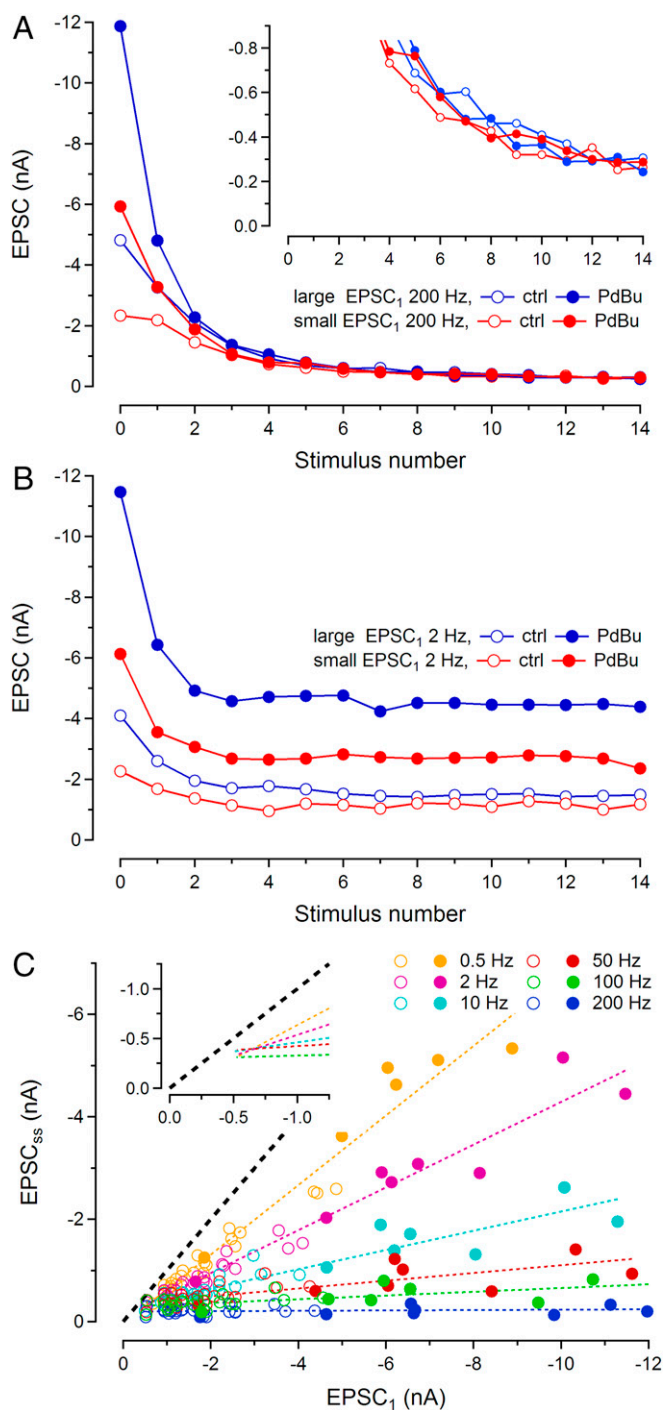


Fig. 3. Dependence of EPSC amplitudes on stimulation frequency. (A) Variability disappears during high-frequency stimulation. Amplitudes of EPSCs during 200-Hz stimulus trains are plotted against stimulus number for two synapses. Blue symbols refer to a synapse with a large EPSC₁ and red symbols to a weak synapse. Open symbols show amplitudes under control conditions and solid ones those after application of 1 μ M PdBu. The curves converge toward similar steady-state values during stimulation. Convergence is not toward zero, but toward a common EPSC_{ss} of about -0.26 nA, as *Inset* shows at expanded y scale. (B) Superpriming is a slow process. Data from the same synapses as shown in A, but now obtained with 2-Hz stimulation, are plotted the same way. At such low frequencies, the heterogeneity among EPSC amplitudes is partially preserved at steady state. (C) Summary of data obtained from 23 synapses in a frequency range from 0.5 Hz to 200 Hz. EPSC_{ss}s (averages of the last 5 EPSCs) are plotted against EPSC₁. Each symbol represents an individual synapse at a given frequency (color coded). Solid symbols are derived from experiments under PdBu, whereas open ones

desensitization, such a model predicts that STD of the SV_s component (reported by the slope of the line fits in Fig. 3C for a given stimulus frequency) is given by $1/(1 + f/f_s)$, where the characteristic frequency f_s is the ratio of the priming rate constant k_{+s} (in units of 1/ISI) and the release probability p_s of the SV_s pool. When trying to fit measured slopes (Fig. 4B) with this relationship and assuming both k_{+s} and p_s to be constant, the results are not compatible with the data (light red dotted curve in Fig. 4B, which we consider the best fit under this constraint). Using a Michaelis–Menten-type function for a frequency-dependent k_{+s} and constant $p_s = 0.5$, however, provides a good fit (Fig. 4B, solid red line). Fig. 4B also includes k_{+s} values, both for the case of a frequency-dependent modulation of the priming rate (solid blue trace) and, for comparison, the constant priming rate of 0.8 s⁻¹ (dotted blue horizontal line). The frequency dependence of k_{+s} , which spans almost a factor of 5 in the frequency range of 0.5–200 Hz, most likely reflects a $[Ca^{2+}]_i$ dependence of the superpriming process. Our values for k_{+s} are very similar to those found for the recovery of the rate of release after pool-depleting stimuli in voltage-clamped calyx of Held terminals (ref. 33, their figure 2C). Together the data show that for stimulus frequencies >20 Hz the contribution of SV_s to EPSC_{ss} is $<10\%$ under our recording conditions due to a combination of slow priming and high p . It should be noted that the pool filling state would be predicted to be even lower than 10%, if p_s were assumed to increase due to facilitation. Below, we show that the priming rate of SV_ns is about six times faster than that of SV_ss, whereas their p is at least three times lower.

Conditioning Stimulation Reveals Properties of Normally Primed SVs.

Considering that under control conditions (absence of PdBu) most of the SV_s component is strongly depressed during ongoing stimulation, the majority of release at steady state must be contributed by SV_ns. Based on the data of Fig. 4B, we expect that even at frequencies as low as 10 Hz the SV_s pool is depleted by more than 80%. This finding opens the possibility to study the properties of SV_ns in isolation with little contamination from SV_ss. For instance, if a 100-Hz stimulus train is applied after 10-Hz conditioning stimulation, we expect to observe during the 100-Hz episode mainly the STP dynamics of SV_ns. This result is illustrated in Fig. 4C, where EPSC train amplitudes during the 100-Hz phase are plotted against stimulus number, both for non-conditioned (symbols with dark colors) and for conditioned trains (symbols with light colors). Average EPSC amplitudes from two groups of synapses ($n = 3$ each) are compared. The first group consists of synapses with relatively large EPSC₁ (blue symbols), whereas for the other group synapses with smaller EPSC₁ were selected (red symbols). The comparison shows that conditioning evens out differences among synapses and turns short-term depression into initial facilitation followed by depression. A similar analysis performed on EPSCs recorded in the presence of PdBu showed that 10-Hz conditioning has a similar effect on PdBu-potentiated synapses ($n = 4$), rendering initial amplitudes more similar and increasing PPR from a control mean value of 0.67 to 1.23.

A conversion of STD into pronounced facilitation by conditioning stimulation was shown previously (41) and interpreted as a reduction in release probability. In the light of the present study, the reduced release probability is seen as a selective depletion of SV_ss. However, even after 10-Hz conditioning, the EPSC trains shown in Fig. 4C may still contain a small SV_s component, which is reduced to approximately one-fifth at steady state for this frequency. Nevertheless, except for the first few EPSCs, any contribution of SV_s during 100-Hz stimulation must be minor, because the SV_s component is reduced to 4% at that frequency. At steady state, the total consumption of SVs is balanced nearly exclusively by recruitment of new SV_ns. We therefore can conclude that SV_ns are primed at a rate of ~ 50 SVs per ISI or 5,000/s (assuming an

represent control conditions. The data for a given frequency are least-squares fitted by straight lines, the slopes of which change strongly with frequency. The line fits for lower frequencies (0.5–100 Hz) intersect at a common point (*Inset* reproduces the line fits without data points). The black dashed line is the identity line (slope = 1), which represents the case that EPSC_{ss} equals EPSC₁ (no depression). Note that even the 0.5-Hz line fit has a slope lower than one.

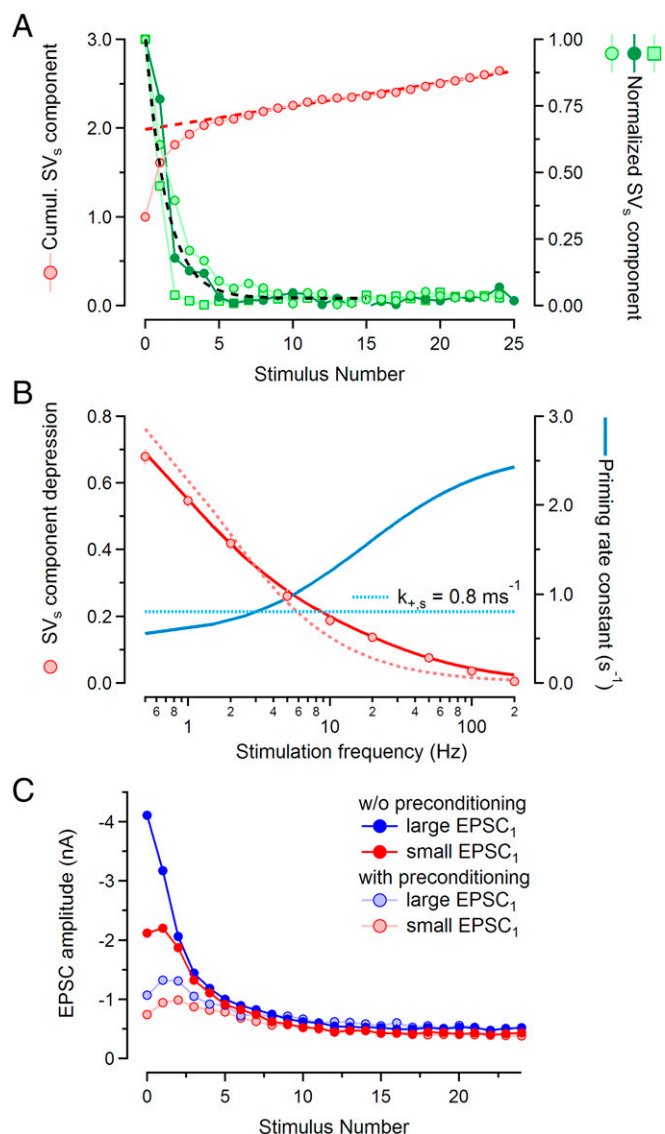


Fig. 4. Isolating the superprimed component of EPSCs. (A) Normalized time courses of contributions from superprimed SVs during 100-Hz trains are plotted against stimulus number (right ordinate). Three examples are shown, each of which was calculated as a difference between average 100-Hz train responses from a set of synapses with large EPSC₁ minus the corresponding average from synapses with small EPSC₁ multiplied by a weighting factor (0.87, 0.822, and 1.06 for the three traces). The lowest trace displays a very rapid decay toward zero, followed by some rebound. This may indicate some residual AMPAR desensitization that is relieved when quantal content is reduced toward steady state. The black dashed curve represents a least-squares fit of an exponential plus baseline to the average of the traces. Superimposed is the cumulative version of the average trace (red circles, left ordinate), together with a line fit to the amplitudes of EPSC₁₁ to EPSC₂₅. (B) Frequency dependence of the steady-state occupancy of the SVs pool. Slopes of line fits from Fig. 3C are plotted against the logarithm of the stimulus frequency (red symbols) together with an adequate fit (solid red curve) and a fit for a fixed priming rate constant of 0.8 s^{-1} (dotted light red curve). Superimposed are the rate constants used for the fits (blue curve, right ordinate). These were either fixed at 0.8 s^{-1} or else calculated with a Michaelis-Menten-type function (basal value 0.5 s^{-1} , maximum value 2.4 s^{-1} , $K_{0.5}$ at 15 Hz). This combination of parameters was used together with $p_s = 0.5$ (SI Text). (C) Conditioning stimulation converts depressing EPSC trains into facilitating ones. EPSC amplitudes during 100-Hz stimulus trains are plotted against stimulus number, for trains both without (symbols with dark colors) and with (symbols with light colors) preceding conditioning stimulation (10 stimuli, 10 Hz). Averages from two groups of synapses (three each) are shown, one with large EPSC₁ (mean = -4.11 nA ,

EPSC amplitude of -0.5 nA contributed by SV_{n,s} and a quantal size of -10 pA in the presence of 1 mM kynurenic acid). Compared with that, a synapse with -2 nA of SV_s contribution to EPSC₁, depressing to about 4%, superprimes only 8 SVs per ISI. In this sense, one can conclude that superpriming is about sixfold slower than normal priming at 100-Hz stimulation. However, p_n , the p of SV_{n,s}, is substantially lower than that of SV_s, as the following consideration shows.

As detailed above, the inverse time constant for the approach of EPSC amplitudes to steady state is the sum of the priming rate constant k_+ (in units of ISIs) and p . Unlike the priming rate constant of SV_s, that of the SV_n pool is large and not negligible, such that $p_n < 1/\tau_n$. Fitting exponentials to the late phases of several sets of 100-Hz EPSC trains conditioned by 10 Hz stimulation, such as those illustrated in Fig. 4C, we obtained an average value for τ_n of 5.4 ISIs. Thus, we can conclude that p_n at steady state is < 0.18 . This value is considerably lower than the estimated p_s of 0.7, as obtained above with the same method. Similar to the estimated p_s , the value of 0.18 may represent a facilitated synapse, such that the initial p_n may well be in the range of 0.1–0.15. In the case that the pool of SV_{n,s} is depleted to only 50%, the initial p_n may be further decreased by one-half. Unfortunately, more accurate values for p_n and $k_{+,n}$ are hard to obtain due to the uncertain residual filling state of the SV_n pool. The important finding, however, remains that at rest $p_n \ll p_s$. During high-frequency stimulation SV_s are rapidly depleted, such that release is supported mainly by SV_{n,s}. Due to facilitation, however, p of these remaining SV_{n,s} will increase as stimulation continues and p_n may increase to about 40% of p_s 's initial value. For this reason, it is hard to distinguish the two components kinetically, unless a detailed analysis is performed. Furthermore, our results suggest that the superpriming rate is $[\text{Ca}^{2+}]_i$ dependent and quite low at low stimulation frequencies (Fig. 4B, blue solid line). Due to rapid decay of residual $[\text{Ca}^{2+}]_i$ after stimulation, $[\text{Ca}^{2+}]_i$ is near baseline during most of the SV_s pool recovery period. Given the basal superpriming rate constant of 0.5 s^{-1} (see above), the time constant of recovery will therefore be in the seconds range. In contrast, priming of SV_{n,s} is fast, at least during high-frequency stimulation. Even if it were slower at rest, substantial refilling of the SV_n pool might occur while $[\text{Ca}^{2+}]_i$ is still elevated after stimulus trains.

Discharge rates in the rodent peripheral auditory pathway are quite high in vivo, even in the absence of acoustic stimulation [median = 10–20 Hz (42)]. Given the low rate of superpriming, this may imply that the pool of SV_s is mostly in a depleted state under physiological conditions. However, two considerations will qualify such a conclusion: (i) Our estimate of eight SV_s being primed per 10 ms (100 Hz) relates to room temperature. Given a strong temperature dependence of the priming process (43), this rate may double at physiological temperatures. (ii) The estimate represents control conditions. Assuming that endogenous modulators have an effect similar to that of PdBu application, the contribution of SV_s may be tripled. In combination, these two effects may lead to a superpriming rate of 48 SV_s per 10 ms or 120 vesicles per ISI at 25 Hz. Thus, effective modulation of synaptic strength and short-term plasticity by SV superpriming may very well occur also under physiological conditions.

Posttetanic Potentiation Shares Properties with PdBu Potentiation and Intrinsic Variability. Posttetanic potentiation is a form of medium-term plasticity (44), during which p (27, 45) and, to a lesser extent, also pool size (15, 46) are increased. It is induced by seconds-long high-frequency stimulation after which synaptic strength is transiently elevated and decays back to control values over several minutes. We hypothesized that PTP may be mediated through a transient increase of the SV_s pool and asked whether PTP shares properties with PdBu potentiation, as well as with the intrinsic heterogeneity of synaptic

blue symbols) and one with smaller EPSC₁ (mean = -2.12 nA , red symbols). Conditioning stimulation reduces differences in synaptic strength among synapses (ratio between EPSC₁ values was 1.94 and 1.45 for 100-Hz trains without and with conditioning 10-Hz stimulation, respectively). It turns STD into facilitation, revealing properties of the contribution of SV_s.

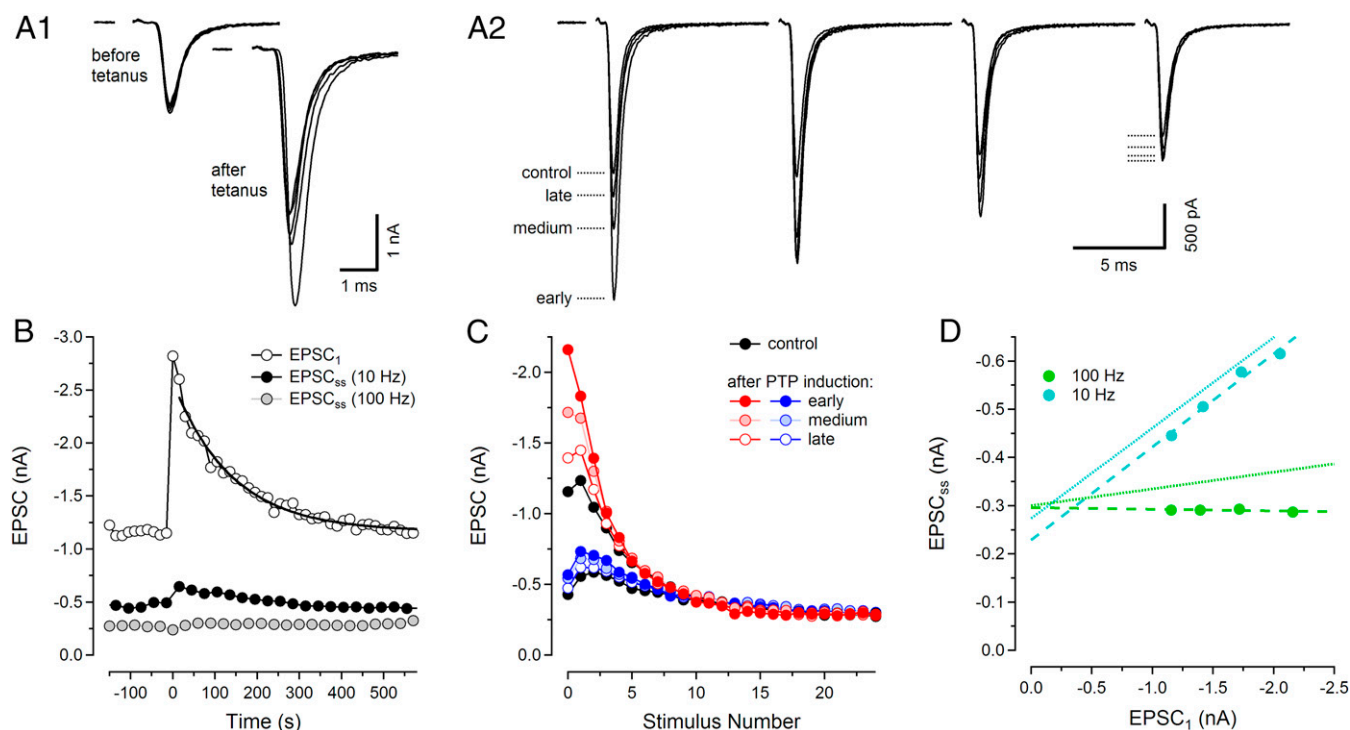


Fig. 5. Posttetanic potentiation of EPSCs can be explained by enhanced superpriming of SVs. (A) EPSCs recorded before and at various time points after induction of PTP, which was induced by 8 s of tetanic stimulation (200 Hz). Before and after PTP induction, 100-Hz trains were delivered every 15 s, alternating with and without conditioning 10-Hz stimulation. (A1) Five individual EPSCs recorded every 60 s before (*Left*) and every 15 s after (*Right*) delivering a 200-Hz tetanus. (A2) Superimposed EPSC trains at 100 Hz stimulation, recorded before and at three time intervals after PTP induction. For clarity, only the initial four EPSCs are shown. EPSC traces are averages of five (before), two (early), three (medium), and two (late) individual trains (exact timing in *SI Text*). (B) Average time course of PTP induction and decay obtained from seven synapses. EPSC₁ amplitudes are plotted against start time of stimulus trains, relative to the time of PTP induction (open circles). An exponential was fitted to the decay time course of the EPSC₁ amplitudes, starting with the second EPSC₁ recorded after PTP induction (thick solid curve). In addition, EPSC_{ss}s are shown for 10 Hz (black circles, average of EPSC₆ to EPSC₁₀) and for 100 Hz (gray circles, average of EPSC₂₁ to EPSC₂₅). (C) Average EPSC amplitudes during 100-Hz stimulation are plotted against stimulus number, for trains both without (red curves and upper black curve) and with (blue curves and lower black curve) preceding conditioning stimulation (10 stimuli, 10 Hz). Averages were calculated for the same early, medium, and late time points as chosen in A2. (D) Average EPSC_{ss}s before and at early, medium, and late time points after PTP induction were calculated as in B and plotted against the corresponding EPSC₁ for both 100 Hz (green circles) and 10 Hz (cyan circles). Superimposed on the data are both regression lines to the scatter plots (dashed lines) and, for comparison, the corresponding line fits from Fig. 3C (dotted lines).

strength as described above. To test this hypothesis, we recorded 100-Hz EPSC trains every 15 s in P15–16 synapses, alternatingly with and without preceding conditioning episodes (consisting of 10 APs at 10 Hz). We then induced PTP by applying 8 s of 200-Hz stimulation before resuming 100-Hz stimulation every 15 s, again with and without preceding 10-Hz conditioning. We found that EPSC₁ amplitudes were potentiated to various degrees. The EPSC₁ of the very first train after PTP induction (7 s after the end of the tetanus) was exceptionally large in some cases and exhibited a slightly increased synaptic delay (Fig. 5A1; also ref. 15). Therefore, we excluded this first train from further analysis. Subsequently, EPSC₁ amplitudes decayed exponentially back to control values. We analyzed nine synapses, in which we were able to complete a total of 19 cycles of PTP induction and recovery. For this dataset, EPSC₁ was potentiated by $115 \pm 10\%$, measured by means of an exponential fit to the EPSC₁ values and back extrapolation of this fit to the end of the PTP-inducing stimulus train.

To analyze other features of PTP, we concentrated on those synapses that showed relatively strong PTP ($\geq 90\%$). These were seven synapses, with 13 cycles of PTP induction and recovery. The average time course of PTP induction and decay is shown in Fig. 5B. PTP is induced at time 0, causing more than doubling of EPSC₁ (average increase = $134 \pm 10\%$, estimated by the procedure described above). After PTP induction, EPSC₁ amplitudes decayed back to control values with a time constant of 155 ± 16 s. For comparison, Fig. 5B also illustrates PTP-induced changes in EPSC_{ss}, for both 100-Hz and 10-Hz stimulation. Contrary to EPSC₁, late EPSCs during 100-Hz trains were hardly changed by PTP induction. This finding is consistent with the

assumption that PTP primarily increases the contribution of SV_s to the EPSC, which are nearly depleted at steady state during 100-Hz trains. The 10-Hz EPSC_{ss} shows only slight potentiation, similar to what was observed for PdBu-induced potentiation of EPSC_{ss} at this frequency and compatible with the slope of the 10-Hz regression line in Fig. 3C.

To visualize changes in short-term plasticity within EPSC trains recorded in potentiated synapses, we calculated average EPSC amplitudes for 100-Hz trains at four time points along the cycles of control—PTP-induction—recovery. The traces are denoted as control (before induction of PTP, black), early (2nd and 3rd train after PTP induction, disregarding the very first EPSC₁), medium (4–6th train), and late (8–10th train) (Fig. 5C). Results from train stimulation both with (Fig. 5C, blue symbols) and without (Fig. 5C, red symbols) preceding 10-Hz conditioning stimulation are shown. In agreement with ref. 15 we found that differences between the EPSC trains measured before and those measured at various time points after PTP induction vanish after three to five stimuli. These findings are consistent with a rapid depletion of SV_s and are similar to those shown in Fig. 3A, where the differences between 200-Hz EPSC trains either were induced by PdBu application or else reflect intrinsic heterogeneity among synapses. Likewise for EPSC trains following conditioning stimulation (Fig. 5C, blue curves) the differences between control and PTP potentiated cases are very much reduced. Also, a sequence of facilitation followed by STD is observed throughout. In contrast, 100-Hz EPSC trains without conditioning stimulation display pronounced STD, when recorded early after PTP induction.

In Fig. 5D we plot EPSC_{ss} vs. EPSC₁ in analogy to Fig. 3C. Here EPSC_{ss} values for the different time points before and after PTP

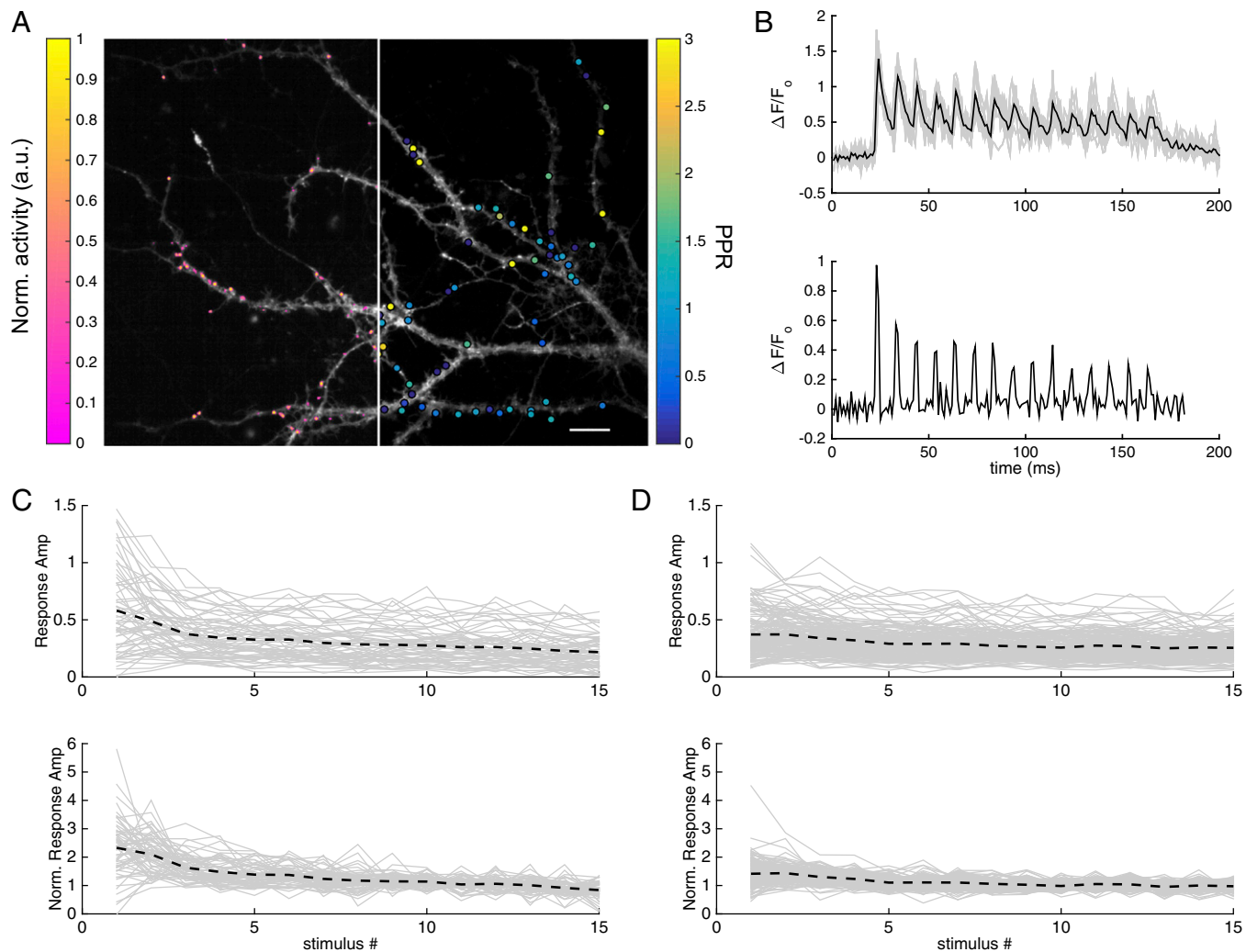


Fig. 6. Imaging glutamate release from hippocampal boutons. (A) Dendrites of hippocampal neurons expressing iGluSnFR were imaged at 100 Hz during which 15 APs were elicited at 10 Hz. *A, Left* is overlaid with a color-coded map showing localization of release onto the dendrites. *A, Right* is overlaid with a map indicating the measured PPR for a given release site. (Scale bar, 10 μm .) (B) Individual normalized fluorescence traces from a single release site in response to the train stimuli are plotted in gray. The mean of 10 repetitions is plotted in black. Responses to individual stimuli overlap due to limited time resolution of the indicator. (*B, Lower*) Deconvolution of the mean fluorescence trace recovers the average response for a given stimulus. (C and D) Peak amplitudes of deconvoluted average responses (shown in B) of all boutons from a representative recording without preconditioning (C) and with preconditioning (D) are plotted in gray. The black dashed line represents the mean of all boutons. In C and D, *Lower*, the response amplitudes are normalized to the mean of the last five responses in the trains.

induction (control, early, medium, and late) are plotted against the respective EPSC₁ both for 100-Hz trains (green symbols) and for 10-Hz trains (cyan symbols). Despite the narrow dynamic range of PTP-induced EPSC amplitude changes, the data points show a clear trend and converge at low values. They intersect at -0.353 nA (dashed lines), similar to the case of Fig. 3C. For comparison, the linear fits for the 10-Hz and 100-Hz data points of Fig. 3C are included (Fig. 5D, dotted lines). This comparison shows that amplitude changes observed during various degrees of PTP are well compatible with the idea that they represent various degrees of superpriming. The finding that PTP is almost absent from EPSC_{ss} even for a stimulus frequency as low as 10 Hz is readily explained by the slow refilling of the SV_s pool (Fig. 4B).

Together our data indicate that four dynamic features of EPSCs evoked by train stimulation, such as (i) pronounced STD during high-frequency stimulation, (ii) a conversion of that STD into a sequence of facilitation followed by STD after a few conditioning stimuli at low frequency, (iii) an equalizing effect of such conditioning stimulation, which reduces differences among synapses and reduces potentiation, and (iv) a requirement of long periods of rest for reconstitution of the original STP pattern, are shared by PdBU potentiation and PTP. Together with the finding that PTP is partially occluded in synapses with

large EPSC₁ (27), our results strongly suggest that both PTP and PdBU potentiation have a common basis.

Heterogeneity Among Individual Active Zones? Heterogeneity with features very similar to those described here was observed among individual boutons in cultured hippocampal neurons by Waters and Smith (47). Using styryl dyes, these authors reported remarkable heterogeneity in the rate of FM1-43 destaining, when measured during 1-Hz stimulation. When stimulating at 10 Hz, however, much less heterogeneity was observed, except for the initial 10–30 responses. These findings recapitulate our results shown in Fig. 3, albeit at lower stimulus frequencies. Waters and Smith suggested that heterogeneity arises from differential partitioning of SVs between the readily releasable pool (RRP) (measured by sucrose stimulation) and the recycling pool (measured by styryl dyes). We hypothesized that a subdivision of the RRP into primed and superprimed components might offer an alternative explanation for their observations. To test this hypothesis, we expressed the novel glutamate sensor iGluSnFR (48) in cultured hippocampal neurons and applied a 10-Hz field stimulation either with or without 1-Hz preconditioning. This method allowed us to measure simultaneously the release of Glu in response

to individual stimuli at up to 186 boutons in a given imaging frame (Fig. 6*A* and *B*). In five experiments, in which the signal-to-noise ratio was large enough to allow quantification of the steady-state response size during 10-Hz stimulation, we observed pronounced heterogeneity among presynaptic boutons [coefficient of variation (CV) = 0.61 ± 0.10 , $n = 5$], when analyzing ratios of the initial responses relative to steady state (Fig. 6*C*). This heterogeneity diminished for responses measured later during the stimulus trains. In contrast to what we observed during train stimulation of calyx synapses, there was substantial heterogeneity also in the size of steady-state responses (note that traces in Fig. 6*C*, *Lower* are normalized with respect to the average of the last five responses). This result probably reflects the well-known size differences of hippocampal boutons and the “scaling” of EPSCs with respect to SV numbers (37). Such differences may be averaged out over the several hundreds of active zones of a given calyx terminal.

In agreement with our findings at calyx synapses, the heterogeneity among boutons of cultured hippocampal neurons regarding their initial responses during stimulation with high-frequency trains is reduced after conditioning with low-frequency trains (CV = 0.37 ± 0.05 , $n = 4$, Fig. 6*D*, compared with 0.61 ± 0.10 , see above), indicating that even at frequencies as low as 1 Hz the putative pool of SV_ss is partially depleted. These results are consistent with the assumption that heterogeneity among boutons is due to a variably sized SV pool that depletes quickly during the first three stimuli of high-frequency trains or during longer-lasting low-frequency stimulation. This pool cannot represent the entire RRP, because depletion of the latter requires several tens of stimuli. Rather, we propose that—as in the calyx—it consists of a small number of SV_ss, which represent only a subset of the entire RRP.

The heterogeneity among individual synaptic boutons is probably averaged out in whole-cell EPSC recordings in hippocampal neurons. Why is heterogeneity nevertheless observed in whole-cell EPSC recordings in MNTB principal neurons? Here, another finding might offer an explanation. As previously reported (38), we observed that p estimates are correlated for neighboring hippocampal boutons. Fig. 6*A*, *Left* shows PPRs as color-coded dots, superimposed onto individual synaptic contacts. A clustering of bright spots (high PPR—low p) in certain regions of the dendritic tree is quite obvious. In Fig. S1 we plot the Pearson correlation coefficient (PCC) of PPRs against distance r_{ij} . To do so, we averaged PCC over all pairs of boutons, which were located within bins of 2.5- μ m widths. A pronounced correlation extends over about 10 μ m with a length constant of 4.1 μ m (Fig. S1). These dimensions are comparable with the total extent of a calyx terminal. Therefore, it is well possible that the signal determining the degree of SV superpriming is similar for all active zones in a given calyx terminal, but differs among calyces, whereas it is averaged out in a widely branched dendritic tree of a cultured hippocampal neuron.

Discussion

Several recent studies described perturbations, either pharmacological or genetic, which change the synaptic release probability in the absence of changes in Ca²⁺ current, [Ca²⁺]_i dynamics, and SV pool sizes (8, 49–51). Whereas changes in the latter parameters are well understood and have been recognized as strong modulators of transmitter release, the mechanisms underlying differences in “intrinsic” release readiness have received less attention. Here, we study three forms of variation in synaptic strength: intrinsic synapse-to-synapse variability; potentiation by the DAG analog PdBu; and PTP, a form of medium-term synaptic plasticity. We show that these three forms of variation display remarkably similar properties, which can be readily and quantitatively explained by the existence of a relatively small subpool of superprimed SVs (SV_ss, ~30%) with high p (~0.5) that is slowly regenerated upon depletion. Following this notion, differences in the size of this pool generate intrinsic heterogeneity among synapses with respect to the mean p , whereas both PdBu and PTP increase the proportion of SV_ss and thereby regulate synaptic strength and plasticity. In contrast, the pool of normally primed SVs (SV_ns) is quite similar in size for individual synapses and remains largely unchanged after PdBu application or PTP induction. SV_ns have low p and are rapidly regenerated after vesicle fusion. We show that high-frequency activity strongly enhances superpriming, most likely via elevated [Ca²⁺]_i. However, even during

100-Hz trains superpriming is much slower than normal priming. This property, combined with high p of about 0.5, leads to the characteristic kinetic STP features described here, which include rapid depletion of the SV_s pool, during both high-frequency stimulation and low-frequency conditioning, leaving behind SV_ns. The latter have low p , which, however, may increase during high-frequency stimulation due to facilitation. Importantly, the majority of SVs consumed during medium- and high-frequency activity are supplied by the SV_ns pool, due to its high priming rate. In contrast, the contribution of SV_ss is dominant only at very low spike rates and at the onset of burst-like activity.

Molecular Mechanisms Regulating Superpriming of SVs. So far, we have interpreted our results in terms of a parallel model that comprises two pools of SVs that are consumed independently with different p and are replenished at different rates. One of the pools is modulated in its size and rate of priming, whereas the other one is static. Alternatively one may assume that SVs undergo a sequential process of initial priming to a state of low p , followed by a slow step of maturation to a state of higher p , as suggested in ref. 52 for cerebellar mossy fiber terminals. If the two states are in a dynamic equilibrium with each other, heterogeneity will arise by different proportions of SVs residing in the superprimed state at rest. This view further suggests that PdBu and PTP shift the population of vesicles toward the state of high p . Such a sequential kinetic scheme is hard to distinguish experimentally from a parallel one, if the first step in the sequence is fast compared with the second one, as is the case at the calyx synapse. However, irrespective of whether superpriming converts normally primed SVs into superprimed ones or else acts on unprimed SVs directly, it is interesting to explore molecular mechanisms under the assumed constraint that PTP, PdBu-induced potentiation, and Rab3 superpriming (32) are mediated by the same or by similar processes. Basu et al. (26) found that interfering with the C1 domain of Munc13 (a target for DAG action) abolished all PdBu-mediated effects and shifted the synapse into a high p state, similar to a PdBu-potentiated synapse. The authors discussed this effect in terms of two conformational states of Munc13, regulated by binding of PdBu (or DAG) to its C1 domain—one state resulting in high p and the other one in low p . Given the fact that Munc13 is a protein with several regulatory domains responsive to DAG, [Ca²⁺]_i, and calmodulin/Ca²⁺ (53), this protein appears as a central hub for modulatory influences on p and superpriming. This view is corroborated by early work on superpriming (32), which implicates the Munc13–Rim–Rab3 interaction as another requirement for this SV maturation process. On the other hand, recent evidence assigns decisive roles to specific isoforms of PKC (6, 28) and PKC-mediated phosphorylation of Munc18 (29) to the induction of PTP. However, assuming that PTP and PdBu-induced potentiation act through the same mechanism (evidence provided here) and given the finding that all effects of PdBu are eliminated by disrupting its interaction with Munc13 (26), we may conclude that Munc13 executes both forms of potentiation by regulating the energy barrier for SV fusion (54). PKC, on the other hand, may enable such regulation through targets, which are part of the release machinery. An example for such enabling reactions is the phosphorylation of Munc18 by PKC (24).

Previous studies at the calyx of Held separated the entire SV population releasable by long-lasting step depolarizations under voltage clamp into two kinetically distinct pools: (i) a slowly releasable pool (SRP) of about 1,500 vesicles, which can be released by such strong stimulation only (34, 55) and contributes little to AP-evoked EPSCs, and (ii) a fast releasable pool (FRP) of similar magnitude, which contributes the vast majority of SVs released during APs. Evidence provided here suggests that SVs of the FRP need to be further subdivided into normally primed and superprimed ones. The SRP likely represents SVs, which have a perfectly assembled release apparatus, but are localized somewhat less favorably with respect to Ca²⁺ channel clusters than FRP vesicles (ref. 56; but see ref. 57). This, together with the considerations above regarding the molecules involved, suggests an attractive scenario for the case that a sequential reaction scheme applies (51): Release-competent SRP vesicles with a fully functional release apparatus undergo a process of positional priming, which moves them closer to Ca²⁺ channels by interaction with the active zone through Rim,

Rab3, and Rim binding protein (58, 59), turning them into FRP vesicles. This process depends on an intact cytoskeleton (33) and happens on the 100-ms timescale. It results in primed SVs with an initial p of 0.1–0.2. Their fast generation and low release probability characterizes them as $SV_{n,s}$. Once interacting with the active zone, the conformational state of Munc13 may slowly shift, which converts $SV_{n,s}$ into $SV_{s,s}$ with a p of ~ 0.5 . The partitioning between primed and superprimed SVs is controlled by DAG and $[Ca^{2+}]_i$ and by interactions of Munc13 with the abovementioned active zone proteins, possibly including GIT (49). In the scenario of a parallel model, these interactions would provide a dynamically changing number of sites for superpriming. Augmentation, a form of synaptic plasticity temporally in between STP and PTP (44, 60), might be represented by the Ca^{2+} -dependent superpriming rate (changing the size of the SV_s pool in synchrony with global $[Ca^{2+}]_i$). PTP, on the other hand, would be brought about by a change in the set point of the SV_n - SV_s partitioning or else by the establishment and disappearance of SV_s sites under the influence of more slowly changing second messengers and by phosphorylation reactions.

Superpriming May Be a Widely Spread Phenomenon Among Excitatory Synapses. The characteristic features of superpriming, as described here, have been observed at glutamatergic synapses in a variety of contexts. Heterogeneity among individual hippocampal synapses has been described both for slice preparations (37, 61) and for cultured hippocampal neurons (38, 62). Hanse and Gustafsson analyzed this heterogeneity at single release sites in the CA1 area of the hippocampus (63, 64). Their findings are reminiscent of the features reported here for calyx synapses. These features include large variability and rapid depletion of a small “preprimed pool” during stimulation, lack of correlation of first response amplitudes with the average release during trains, and accelerated priming during trains. Using styryl dyes and cultured hippocampal neurons, strong heterogeneity of release was observed among individual boutons, when stimulating at 1 Hz, whereas synaptic strength was more uniform, with some of the remaining heterogeneity disappearing after a few stimuli, when stimulating at 10 Hz (47). Ishiyama et al. (65) describe a decrease in p in granule cell to basket cell synapses of the cerebellum of Munc13-3^{-/-} mice. They interpret their observations as a loss of a superpriming action of Munc13-3. A small number of release sites with especially high release probability were postulated to mediate release during low-frequency

stimulation at the neuromuscular junction (66). Taken together, these results suggest that superpriming is a widely spread mechanism among excitatory synapses. It provides enhanced synaptic strength for a few initial APs during a burst of activity. This enhancement happens only when AP bursts have been preceded by periods of quiescence of a few hundred milliseconds. Its impact on network properties can be modulated by slow neurotransmitter systems.

Materials and Methods

Slice Preparation and Electrophysiology. Juvenile, posthearing (P13–16) Wistar rats of either sex were used. All experiments complied with the German Protection of Animals Act and with the guidelines for the welfare of experimental animals issued by the European Communities Council Directive. Brainstem slices were prepared as previously described (35). Whole-cell patch-clamp recordings were made from principal neurons of the MN1B, using an EPC-10 amplifier controlled by “Pulse” software (HEKA Elektronik). Action potentials were elicited by afferent fiber stimulation. All experiments were carried out at room temperature in the presence of 1 mM kynurenic acid to minimize AMPAR saturation and desensitization (*SI Materials and Methods*).

Statistical Analysis and Model Calculations. Offline analysis was performed using “Igor Pro” (Wavemetrics). Original data are presented as mean \pm SEM. SDs of parameters are given as provided by Igor Pro curve-fitting programs. For derived quantities (products, ratios, etc.) SEM was calculated assuming Gaussian error propagation.

Optical Measurements. Primary hippocampal neuron cultures were prepared from 1-d-old Wistar rats according to the regulations of the Max Planck Society. Calcium phosphate-mediated transfection of neurons with iGluSnFR (Addgene plasmid 41732) was performed at 3 d in vitro (DIV) and experiments were performed at DIV 14–21. Images were acquired at 100 Hz with a Zyla 5.5 sCMOS camera (Andor Technology). Action potentials were elicited by field stimulation. All experiments were performed at room temperature (*SI Materials and Methods*).

ACKNOWLEDGMENTS. We thank Manfred Lindau for valuable discussions and comments on the manuscript, F. Würriehausen for expert advice on programming, and I. Herfort for excellent technical assistance. This work was supported by the Cluster of Excellence and Center for Nanoscale Microscopy and Molecular Physiology of the Brain (E.N., A.W., and H.T.), the European Commission (EUROSPIN, FP7HEALTHF22009241498; to E.N.), and the Max Planck Society (E.N.).

- Zucker RS, Regehr WG (2002) Short-term synaptic plasticity. *Annu Rev Physiol* 64:355–405.
- Chanda S, Xu-Friedman MA (2011) Excitatory modulation in the cochlear nucleus through group I metabotropic glutamate receptor activation. *J Neurosci* 31(20):7450–7455.
- Billups B, Graham BP, Wong AY, Forsythe ID (2005) Unmasking group III metabotropic glutamate autoreceptor function at excitatory synapses in the rat CNS. *J Physiol* 565(Pt 3):885–896.
- Brenowitz S, Trussell LO (2001) Minimizing synaptic depression by control of release probability. *J Neurosci* 21(6):1857–1867.
- Wang T, Rusu SI, Hruskova B, Turecek R, Borst JG (2013) Modulation of synaptic depression of the calyx of Held synapse by GABA(B) receptors and spontaneous activity. *J Physiol* 591(19):4877–4894.
- de Jong AP, Fioravante D (2014) Translating neuronal activity at the synapse: Presynaptic calcium sensors in short-term plasticity. *Front Cell Neurosci* 8:356.
- Junge HJ, et al. (2004) Calmodulin and Munc13 form a Ca^{2+} sensor/effector complex that controls short-term synaptic plasticity. *Cell* 118(3):389–401.
- Chang S, et al. (2015) Complexin stabilizes newly primed synaptic vesicles and prevents their premature fusion at the mouse calyx of Held synapse. *J Neurosci* 35(21):8272–8290.
- Südhof TC (2012) The presynaptic active zone. *Neuron* 75(1):11–25.
- Abbott LF, Varela JA, Sen K, Nelson SB (1997) Synaptic depression and cortical gain control. *Science* 275(5297):220–224.
- Cook DL, Schwandt PC, Grande LA, Spain WJ (2003) Synaptic depression in the localization of sound. *Nature* 421(6918):66–70.
- Banitt Y, Martin KA, Segev I (2007) A biologically realistic model of contrast invariant orientation tuning by thalamocortical synaptic depression. *J Neurosci* 27(38):10230–10239.
- Mongillo G, Barak O, Tsodyks M (2008) Synaptic theory of working memory. *Science* 319(5869):1543–1546.
- von der Malsburg C, Bienenstock E (1986) Statistical coding and short-term synaptic plasticity: A scheme for knowledge representation in the brain. *Disordered Systems and Biological Organization*, eds Bienenstock E, Fogelman-Soulié F, Weisbuch G (Springer, Berlin), pp 247–272.
- Habets RL, Borst JG (2007) Dynamics of the readily releasable pool during post-tetanic potentiation in the rat calyx of Held synapse. *J Physiol* 581(Pt 2):467–478.
- Castro-Alamancos MA, Connors BW (1996) Short-term plasticity of a thalamocortical pathway dynamically modulated by behavioral state. *Science* 272(5259):274–277.
- de Jong AP, Verhage M (2009) Presynaptic signal transduction pathways that modulate synaptic transmission. *Curr Opin Neurobiol* 19(3):245–253.
- Lee SH, Dan Y (2012) Neuromodulation of brain states. *Neuron* 76(1):209–222.
- Takahashi T, Forsythe ID, Tsujimoto T, Barnes-Davies M, Onodera K (1996) Presynaptic calcium current modulation by a metabotropic glutamate receptor. *Science* 274(5287):594–597.
- Takahashi T (2005) Dynamic aspects of presynaptic calcium currents mediating synaptic transmission. *Cell Calcium* 37(5):507–511.
- Isaacson JS (1998) GABAB receptor-mediated modulation of presynaptic currents and excitatory transmission at a fast central synapse. *J Neurophysiol* 80(3):1571–1576.
- Hori T, Takai Y, Takahashi T (1999) Presynaptic mechanism for phorbol ester-induced synaptic potentiation. *J Neurosci* 19(17):7262–7267.
- Lou X, Korogod N, Brose N, Schneggenburger R (2008) Phorbol esters modulate spontaneous and Ca^{2+} -evoked transmitter release via acting on both Munc13 and protein kinase C. *J Neurosci* 28(33):8257–8267.
- Wierda KD, Toonen RF, de Wit H, Brussaard AB, Verhage M (2007) Interdependence of PKC-dependent and PKC-independent pathways for presynaptic plasticity. *Neuron* 54(2):275–290.
- Wu XS, Wu LG (2001) Protein kinase c increases the apparent affinity of the release machinery to Ca^{2+} by enhancing the release machinery downstream of the Ca^{2+} sensor. *J Neurosci* 21(20):7928–7936.
- Basu J, Betz A, Brose N, Rosenmund C (2007) Munc13-1 C1 domain activation lowers the energy barrier for synaptic vesicle fusion. *J Neurosci* 27(5):1200–1210.
- Korogod N, Lou X, Schneggenburger R (2005) Presynaptic Ca^{2+} requirements and developmental regulation of posttetanic potentiation at the calyx of Held. *J Neurosci* 25(21):5127–5137.
- Fioravante D, et al. (2014) Protein kinase C is a calcium sensor for presynaptic short-term plasticity. *eLife* 3:e03011.
- Genc O, Kochubey O, Toonen RF, Verhage M, Schneggenburger R (2014) Munc18-1 is a dynamically regulated PKC target during short-term enhancement of transmitter release. *eLife* 3:e01715.
- Fioravante D, Regehr WG (2011) Short-term forms of presynaptic plasticity. *Curr Opin Neurobiol* 21(2):269–274.

31. Grande G, Wang LY (2011) Morphological and functional continuum underlying heterogeneity in the spiking fidelity at the calyx of Held synapse in vitro. *J Neurosci* 31(38):13386–13399.
32. Schlüter OM, Basu J, Südhof TC, Rosenmund C (2006) Rab3 superprimes synaptic vesicles for release: Implications for short-term synaptic plasticity. *J Neurosci* 26(4):1239–1246.
33. Lee JS, Ho WK, Neher E, Lee SH (2013) Superpriming of synaptic vesicles after their recruitment to the readily releasable pool. *Proc Natl Acad Sci USA* 110(37):15079–15084.
34. Sakaba T, Neher E (2001) Calmodulin mediates rapid recruitment of fast-releasing synaptic vesicles at a calyx-type synapse. *Neuron* 32(6):1119–1131.
35. Taschenberger H, von Gersdorff H (2000) Fine-tuning an auditory synapse for speed and fidelity: Developmental changes in presynaptic waveform, EPSC kinetics, and synaptic plasticity. *J Neurosci* 20(24):9162–9173.
36. Debanne D, Guérineau NC, Gähwiler BH, Thompson SM (1996) Paired-pulse facilitation and depression at unitary synapses in rat hippocampus: Quantal fluctuation affects subsequent release. *J Physiol* 491(Pt 1):163–176.
37. Dobrunz LE, Stevens CF (1997) Heterogeneity of release probability, facilitation, and depletion at central synapses. *Neuron* 18(6):995–1008.
38. Murthy VN, Sejnowski TJ, Stevens CF (1997) Heterogeneous release properties of visualized individual hippocampal synapses. *Neuron* 18(4):599–612.
39. Schneggenburger R, Meyer AC, Neher E (1999) Released fraction and total size of a pool of immediately available transmitter quanta at a calyx synapse. *Neuron* 23(2):399–409.
40. Neher E (2015) Merits and limitations of vesicle pool models in view of heterogeneous populations of synaptic vesicles. *Neuron* 87(6):1131–1142.
41. Müller M, Goutman JD, Kochubey O, Schneggenburger R (2010) Interaction between facilitation and depression at a large CNS synapse reveals mechanisms of short-term plasticity. *J Neurosci* 30(6):2007–2016.
42. Kopp-Scheinflug C, Tolnai S, Malmierca MS, Rübsamen R (2008) The medial nucleus of the trapezoid body: Comparative physiology. *Neuroscience* 154(1):160–170.
43. Kushmerick C, Renden R, von Gersdorff H (2006) Physiological temperatures reduce the rate of vesicle pool depletion and short-term depression via an acceleration of vesicle recruitment. *J Neurosci* 26(5):1366–1377.
44. Magleby KL (1979) Facilitation, augmentation, and potentiation of transmitter release. *Prog Brain Res* 49:175–182.
45. Magleby KL, Zengel JE (1976) Augmentation: A process that acts to increase transmitter release at the frog neuromuscular junction. *J Physiol* 257(2):449–470.
46. Lee JS, Kim MH, Ho WK, Lee SH (2008) Presynaptic release probability and readily releasable pool size are regulated by two independent mechanisms during post-tetanic potentiation at the calyx of Held synapse. *J Neurosci* 28(32):7945–7953.
47. Waters J, Smith SJ (2002) Vesicle pool partitioning influences presynaptic diversity and weighting in rat hippocampal synapses. *J Physiol* 541(Pt 3):811–823.
48. Marvin JS, et al. (2013) An optimized fluorescent probe for visualizing glutamate neurotransmission. *Nat Methods* 10(2):162–170.
49. Montesinos MS, et al. (2015) Presynaptic deletion of GIT proteins results in increased synaptic strength at a mammalian central synapse. *Neuron* 88(5):918–925.
50. Körber C, et al. (2015) Modulation of presynaptic release probability by the vertebrate-specific protein mover. *Neuron* 87(3):521–533.
51. Yao L, Sakaba T (2010) cAMP modulates intracellular Ca²⁺ sensitivity of fast-releasing synaptic vesicles at the calyx of Held synapse. *J Neurophysiol* 104(6):3250–3260.
52. Hallermann S, et al. (2010) Bassoon speeds vesicle reloading at a central excitatory synapse. *Neuron* 68(4):710–723.
53. Wojcik SM, Brose N (2007) Regulation of membrane fusion in synaptic excitation-secretion coupling: Speed and accuracy matter. *Neuron* 55(1):11–24.
54. Schotten S, et al. (2015) Additive effects on the energy barrier for synaptic vesicle fusion cause supralinear effects on the vesicle fusion rate. *eLife* 4:e05531.
55. Sakaba T (2006) Roles of the fast-releasing and the slowly releasing vesicles in synaptic transmission at the calyx of Held. *J Neurosci* 26(22):5863–5871.
56. Wadel K, Neher E, Sakaba T (2007) The coupling between synaptic vesicles and Ca²⁺ channels determines fast neurotransmitter release. *Neuron* 53(4):563–575.
57. Wölfel M, Lou X, Schneggenburger R (2007) A mechanism intrinsic to the vesicle fusion machinery determines fast and slow transmitter release at a large CNS synapse. *J Neurosci* 27(12):3198–3210.
58. Dulubova I, et al. (2005) A Munc13/RIM/Rab3 tripartite complex: From priming to plasticity? *EMBO J* 24(16):2839–2850.
59. Han Y, Kaeser PS, Südhof TC, Schneggenburger R (2011) RIM determines Ca²⁺ channel density and vesicle docking at the presynaptic active zone. *Neuron* 69(2):304–316.
60. Garcia-Perez E, Wesseling JF (2008) Augmentation controls the fast rebound from depression at excitatory hippocampal synapses. *J Neurophysiol* 99(4):1770–1786.
61. Hessler NA, Shirke AM, Malinow R (1993) The probability of transmitter release at a mammalian central synapse. *Nature* 366(6455):569–572.
62. Rosenmund C, Clements JD, Westbrook GL (1993) Nonuniform probability of glutamate release at a hippocampal synapse. *Science* 262(5134):754–757.
63. Hanse E, Gustafsson B (2001) Vesicle release probability and pre-primed pool at glutamatergic synapses in area CA1 of the rat neonatal hippocampus. *J Physiol* 531(Pt 2):481–493.
64. Hanse E, Gustafsson B (2001) Factors explaining heterogeneity in short-term synaptic dynamics of hippocampal glutamatergic synapses in the neonatal rat. *J Physiol* 537(Pt 1):141–149.
65. Ishiyama S, Schmidt H, Cooper BH, Brose N, Eilers J (2014) Munc13-3 superprimes synaptic vesicles at granule cell-to-basket cell synapses in the mouse cerebellum. *J Neurosci* 34(44):14687–14696.
66. Cano R, Ruiz R, Shen C, Tabares L, Betz WJ (2012) The functional landscape of a presynaptic nerve terminal. *Cell Calcium* 52(3–4):321–326.
67. Traynelis SF (1998) Software-based correction of single compartment series resistance errors. *J Neurosci Methods* 86(1):25–34.